

# Glass-molded optical interposers for wafer scale photonic integrated circuit packaging in 800G modules and co-packaged optics

M. Ackermann<sup>a</sup>, B. Shen<sup>a</sup>, F. Merget<sup>a,b</sup>, M. Wolz<sup>c</sup>, J. Witzens<sup>\*,a,b</sup>

<sup>a</sup>Institute of Integrated Photonics, RWTH Aachen, 52074 Aachen, Germany;

<sup>b</sup>aiXscale Photonics UG, Virchowstr. 14, 50935 Köln, Germany;

<sup>c</sup>GD Optical Competence GmbH, Herborner Strasse 7-9, 35764 Sinn, Germany

## ABSTRACT

We report on glass-molded micro-optical interposers for single-mode fiber-to-PIC coupling fabricated in parallel by isothermal molding of 1-inch glass plates yielding over 100 arrays of 8 lenses each. Excess losses between PIC and single-mode fiber are below 1 dB. In addition to allowing a narrow package footprint, beam transformation maps mode profiles between fibers and surface couplers, and, in case of grating couplers, can adapt the light incidence angle on a wavelength-specific basis, facilitating packaging of PICs in CWDM and LAN-WDM modules. The interposers can be further extended to support polarization management and isolation by coating with polarization selective thin film stacks in MacNeille configuration, as well as wavelength multiplexing by coating with dichroic stacks. Using this technique, over 256 bidirectional transceiver channels can be packaged in the footprint of a single reticle.

**Keywords:** Optical interposer, optical packaging, fiber-to-PIC coupling, co-packaged optics, isothermal glass molding

## 1. INTRODUCTION AND BASIC CONCEPTS

Optical subassembly and backend packaging make up for 30% to 90% of the total manufacturing cost of optical transceivers and are thus a major cost driver limiting the architectural levels at which silicon photonics (SiP) technology can be deployed.<sup>1</sup> To fully exploit the potential created by chip-scale CMOS compatible fabrication of complex photonic integrated circuits,<sup>2</sup> an equally scalable and low-cost packaging technology is necessary at the wafer-scale, that is capable of supporting the high fiber count required for emerging form factors such as 800G modules and co-packaged optics (CPO).<sup>3</sup> Aperture sizes of vertical cavity surface-emitting lasers (VCSELs) and large area detectors (LADs) have also been shrinking as serial data rates have been rising to support required modulation bandwidths.<sup>4</sup> Single mode VCSELs are further seen as an alternative to increase the reach of low cost optical modules.<sup>5</sup> As a result, tighter requirements on the subassembly alignment tolerances create a need for high-precision micro-optics manufactured at a low enough cost with a coefficient of thermal expansion (CTE) matched to that of the utilized silicon or ceramic submounts.

We report on glass interposers that can be molded, surface treated, and assembled at the wafer scale, serving to fiber couple surface emitting photonic integrated circuits (PICs) as well as VCSELs and LADs, providing a low-cost and scalable solution for the packaging of CPO for top-of-the-rack (TOR) switches and datacom modules. Besides providing compact light routing and fiber coupling capabilities, they have been engineered to support wavelength division multiplexing (WDM), polarization management, and optical isolation. By leveraging the degrees of freedom afforded by mold based shaping, functional elements such as reflective surfaces, mechanical attachment surfaces, spacers and alignment fiducials can be integrated in the same glass piece without increasing processing time. This differentiates this fabrication process from other methods used to manufacture dense lens arrays such as grey-scale lithography<sup>6</sup> and significantly reduces the number of piece parts required to manufacture complex interposers.

### 1.1 Isothermal glass molding

Isothermal glass molding is a technique that consists in imprinting the inverse topology of a mold onto a glass wafer with a pressure in the order of tens of kilonewton at an elevated temperature that is identical in the glass and in the mold and is in the order of the glass transition temperature.<sup>7</sup> Both top and bottom surfaces can be patterned with structures that maintain optical quality surfaces. The cycling time of the glass press is limited by the requirement of heating up and cooling down the entire process chamber, in our case ~20 minutes. Non-isothermal glass molding can potentially increase throughput

\*jwitzens@aixscalephotonics.com; phone +49 241 80 20021; iph.rwth-aachen.de

due to the possibility of pipelining the heating, pressing and cooling stages. It does, however, present additional restrictions in terms of the features that can be molded due to the thermal gradients in the glass and requires more expensive equipment. Since we are currently molding up to a 1000 lenses in parallel into a 1" by 1" glass wafer and have the ability to further parallelize the process, the developed isothermal molding process is compatible with very high volumes. Currently fabricated microlenses are grouped in arrays of four overlapping lenses having each a radius of curvature (ROC) of 220  $\mu\text{m}$  and spaced by 250  $\mu\text{m}$  from each other. White light interferometry reveals a manufacturing precision with a global deviation from target below 20 nm and a local root mean square roughness in the single-digit nanometer range. These groups of lenses are arranged on the glass wafer to allow simple dicing and handling thereafter. Their density is also constrained by the overall interposer functionality described in the following and is thus not an intrinsic limitation of the glass molding process itself.

### 1.2 Basic interposer building block

Figure 1 shows the simplest glass interposer configuration. As represented in the schematic in Fig. 1(a), two identical glass pieces, with four lenses each spaced 250  $\mu\text{m}$  apart, are joined together with ultraviolet (UV)-curable index-matched epoxy. These interposer building blocks are obtained by dicing of the glass wafer in which they have been molded in parallel. Attachment surfaces allow the mounting of the interposer on top of a PIC or an optical sub-mount, as well as attachment of a fiber array (FA). The group of lenses are recessed by 400  $\mu\text{m}$  so that the emitting/receiving surface of the PIC or FA are close to the focal plane of the lenses. Consequently, the light, with beam path represented by the red arrows inside of the interposer, is collimated inside it. A flat surface tilted 45° relative to the reference planes of the lenses acts as a mirror that redirects the light across a 90° angle by total internal reflection. Routing of the light on a Cartesian grid relaxes the tolerance on the building block thickness, given by the distance between the top and bottom mold during the forming process, as it then no longer influences the position at which the beam exits the structure relative to the output lens array. Moreover, the beams are expanded to a mode field diameter in the order of a hundred micrometer at the junction between the glass pieces, placing the assembly tolerances well within the reach of high-throughput pick-and-place assembly.

The outer dimensions of the interposer are labeled in Fig. 1(b). With surface 1 attached to the PIC, the height of the subassembly can be kept below 2.66 mm, compatible with low-rise form factors. The 2 mm structure width (along the direction in which the lenses are placed next to each other) was chosen to be compatible with standard FAs. Together with requirements for reliable epoxy based attachment, this constrains the footprint of the current configuration. To connect more than 4 fibers to a single PIC with parallel optical interfaces, interposer blocks as depicted in Fig. 1 can be left attached to each other in a bar containing several groups of four lenses and transferred together to the optical subassembly.

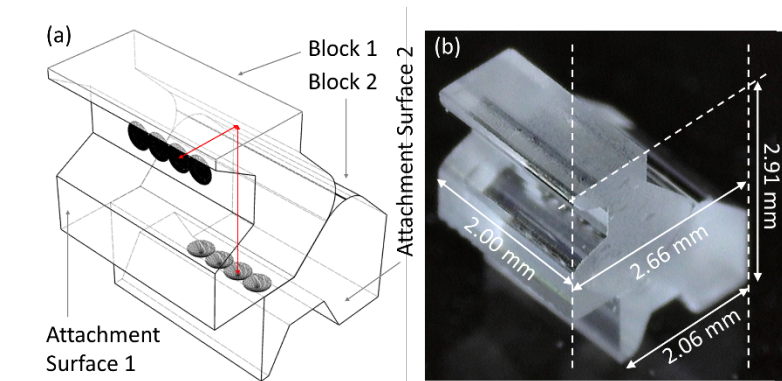


Figure 1. Basic interposer configuration. (a) CAD drawing in perspective view. The light path inside the interposer is shown in red. (b) Photograph of the assembled interposer.

## 2. INTERPOSER MODEL AND MEASUREMENTS

### 2.1 Zemax Optic Studio model

The performance of the interposer was modeled with ray-tracing using the Optic Studio software from Zemax. Fresnel propagation is taken into account by using the physical optical propagation tool (POP). A Gaussian beam corresponding to the emission of a single-mode fiber (Corning SMF-28) at 1310 nm was launched from the attachment plane on one side

of the interposer and assumed to be collected by another SMF at the other attachment plane. Coupling to the second fiber was evaluated by a scalar mode overlap with the optical fiber mode.

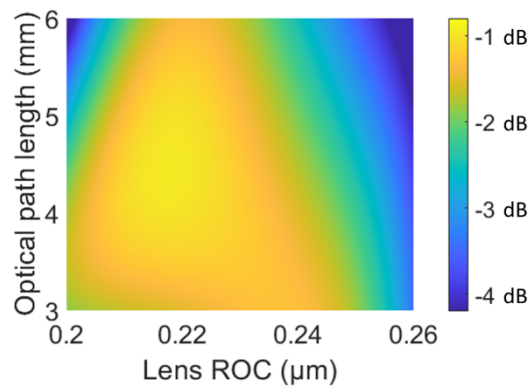


Figure 2. Interposer ILs as a function of the total light path length inside the glass and of the radius of curvature of the lenses, assumed to be identical at the input and at the output. Light is coupled between standard SMFs. Perfect anti-reflection coatings are assumed to be applied on the interposer lenses in the simulation.

Figure 2 shows the modeled insertion losses (ILs) as a function of the path length travelled by the ray inside the glass, assuming the input and output lenses to be identical. The optimum lens radius corresponds to a focal length that is slightly below the 400 μm recess depth defining the distance between the lenses to the PIC/FA, since a slight amount of refocusing inside the glass is required to compensate for beam diffraction. ILs of better than 1 dB are limited by the lens aberration and can be improved further by utilizing an aspherical lens shape.

## 2.2 Lens quality assessment

The quality of individual lenses was inspected with two methods using a white light interferometer and a confocal scanning laser microscope, covering the lenses' center region with a diameter of 50 μm and 150 μm, respectively. Deviations from the best fitted sphere, with a radius of 219.66 μm very close to the designed 220 μm, were better than ±20 nm. To verify the optical quality of the lens surface, the residual roughness was also extracted by subtracting the smoothed large scale deviations by applying a spatial filter. Its arithmetic mean deviation  $R_a$  was found to be 7.4 nm after applying a filter with a 60 μm lowpass cutoff.

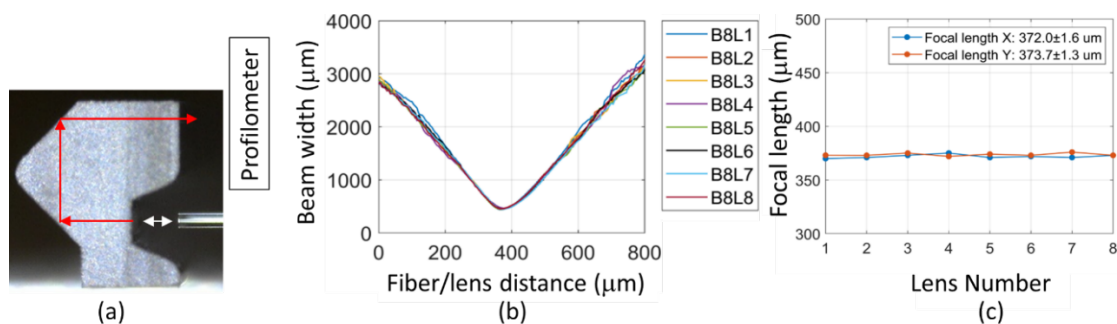


Figure 3. Measurement using a cleaved fiber and a beam profiler to optically characterize the lenses. (a) Measurement setup. (b) Beam width versus fiber-to-lens distance and (c) extracted focal length taking the 12.7 mm free-space propagation length between the interposer and the beam profiler into account. While the recess formed in the glass block to position the lens is clearly visible in (a), the lens itself is positioned deeper in the structure along the axis of the camera and is not resolved.

To verify the functionality and the reproducibility of the molded lenses, measurements were performed on an interposer bar comprising eight parallel lenses. Figure 3(a) shows the measurement setup. A cleaved fiber is oriented along the optical axis of the lens and positioned at different distances by translating it along the white arrow. After being transformed by the lens, light is reflected by the two flat facets, forming a corner reflector in this configuration. After exiting the glass block, light propagates by an additional 12.7 mm before reaching a beam profiler from which the mode field diameter

(MFD) is extracted. Panel (b) shows the beam width vs. the fiber-to-lens distance. The curves for the eight investigated lenses almost perfectly overlay, showing excellent repeatability even though these lenses were shaped from places on the mold that were individually machined. The extracted focal lengths are presented in panel (c) for both transverse axes. There is no significant astigmatism and the lenses present very similar properties. The focal length of the lenses is slightly below  $400\ \mu\text{m}$ , as targeted, so that a mode profile imaged from the attachment plane results in a slight refocusing inside the glass, as required to compensate diffraction.

### 2.3 Single-mode fibers coupled through interposer

Figure 4 shows the transmission measured between two SMFs that are coupled by the interposer and can be each freely aligned along six axes. The measurement setup is shown in Fig. 4(a). The ILs of the four channels, each corresponding to a pair of lenses, are about 1.8 dB. In addition to the  $\sim 1\ \text{dB}$  ILs determined by ray tracing,  $\sim 0.72\ \text{dB}$  are accounted for by the four glass-air interfaces, since the building blocks have not yet been provided with an anti-reflective coating.

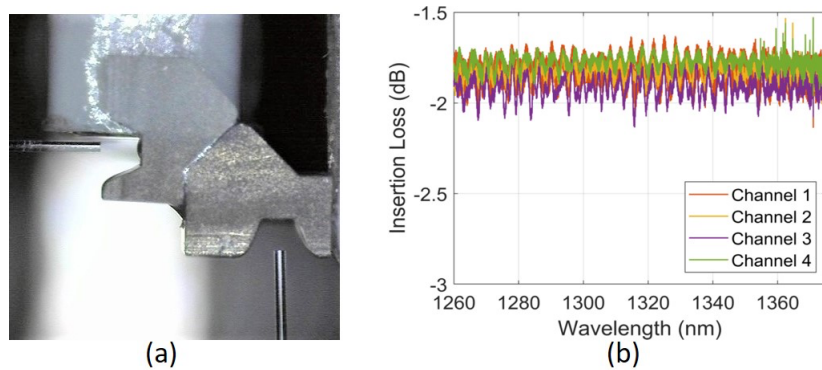


Figure 4. Transmission between independent fibers coupled by the interposer. (a) Measurement setup in which both fibers are freely aligned along six axes. (b) Measured insertion losses across the O-band for all four lens pairs.

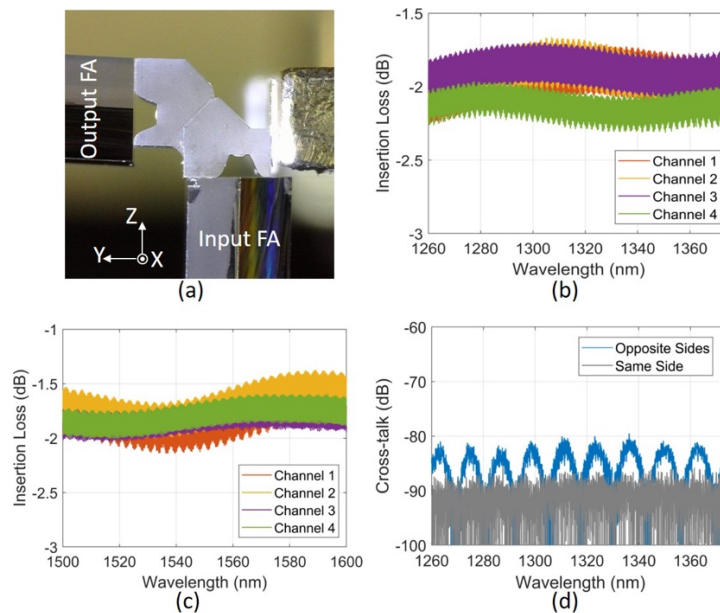


Figure 5. Transmission and cross-talk measurements for interposer with FAs. (a) Measurement setup. Fibers are embedded into FAs on both sides of the interposer and the surface of the FAs aligned flush with the interposer surface, imposing a rigid arrangement between the fibers. ILs in (b) the O- and (c) C-bands. (d) Cross-talk between fibers coupled to channel 1 and channel 2, either on the same side (black) or on opposite sides (blue) of the interposer.

Transmission and cross-talk measurements between SMFs rigidly embedded into FAs with a 250  $\mu\text{m}$  pitch coinciding with that of the interposer lenses are shown in Fig. 5. The facets of the FAs have a polished surface nominally angled by  $2.4^\circ$ , close to the emission angle of 1310 nm grating couplers (GCs) we have developed. The measurement setup is shown in Fig. 5(a). The facets of the FAs are flush with the attachment surfaces of the interposer, with which they are in mechanical contact. In Fig. 5(b), we can see that the ILs of the interposer with FAs are slightly worse than those with freely aligned fibers. This is due to the facets of the fibers embedded in the FAs being constrained to lie exactly in the interposer's attachment planes, showing that the fabricated lenses are not yet ideal for this configuration and should be retargeted to recover this small drop in ILs (it is visible in Fig. 4 that one of the freely moveable fibers has its facet slightly inside the recessed region of the interposers, revealing that the focal lengths of the lenses are slightly too short to be optimum). The positioning of the lenses relative to each other on a given block is better than  $\pm 1 \mu\text{m}$  and leads to negligible ILs on its own, but could also stack up with fiber positioning tolerances in the FAs. The pronounced ripple in the spectra has a free spectral range that could be attributed to the optical path length between the two FA facets. ILs between coupled fibers remain better than 2 dB over the entire O- and C-bands, see Figs. 5(b) and 5(c). Cross-talk between adjacent channels on either the opposite sides or the same side of the interposer is extremely low and remains below -80 dB.

Figure 6 shows the alignment tolerance at channel 1 at a wavelength of 1310 nm (corresponding axes are indicated in Fig. 5(a)). The -1 dB and -3 dB alignment tolerances of the interposer are about  $\pm 2 \mu\text{m}$  and  $\pm 4 \mu\text{m}$ , respectively, as expected from the MFD of the single mode fibers.

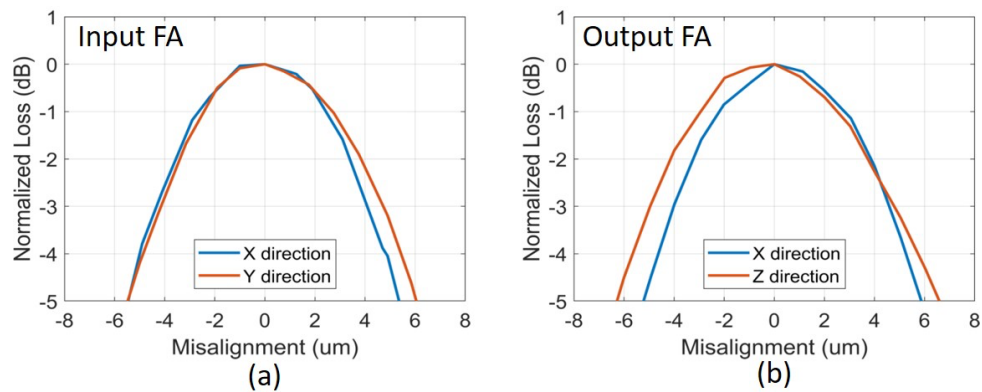


Figure 6. Alignment tolerance at channel 1 of the interposer with fibers embedded in FAs at a wavelength of 1310 nm. (a) Alignment tolerances of the input FA in the X- (blue) and Y-directions (red) and (b) of the output FA in the X- (blue) and Z-directions (red).

## 2.4 PIC coupled through interposer to FA

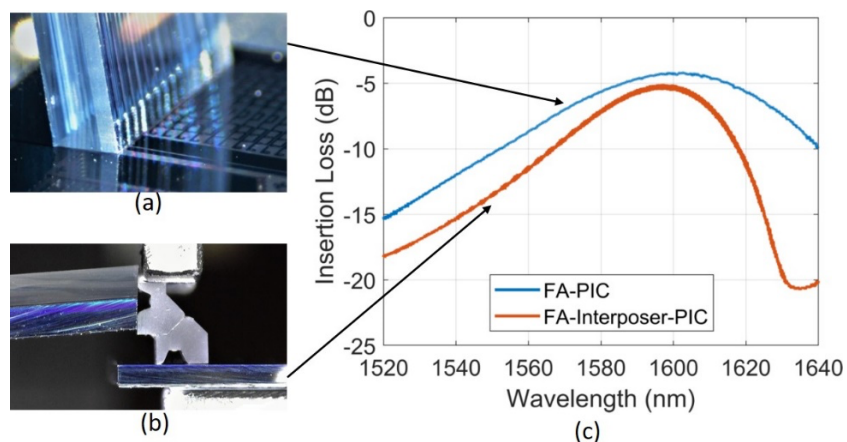


Figure 7. Measurement setup for coupling of an FA to a PIC via a GC, without (a) and with (b) interposer. (c) Transmission spectra without (blue) and with (red) interposer.

The measurement setup used to investigate the coupling of a FA to a PIC via GCs and the interposer is shown in Fig. 7(b). Reference data is collected by directly positioning the FA onto the PIC, see Fig. 7(a). The FA used here is also populated with standard single-mode fibers with a pitch of 250  $\mu\text{m}$ , its facet is however polished with a 6° angle. The PIC was fabricated in a 220 nm thick silicon-on-insulator (SOI) device layer in the standard SiP process at Singapore’s Advanced Micro Foundry (AMF). Two pairs of GCs are used on the PIC to form two waveguide loops, providing a total of four optical ports to couple to, with a pitch matched to that of the interposer and of the FA.

Transmission spectra recorded between two FA ports coupling to a waveguide loop via GCs without (blue curve) and with (red curve) interposer are shown in Fig. 7(c). In order to show the losses per interface, the total fiber-to-fiber insertion losses were divided by two. For the case without interposer, the minimum loss is 4.2 dB at a wavelength of 1602.6 nm, while for the case with interposer the minimum loss is 5.1 dB at a wavelength of 1597.2 nm, corresponding to an excess loss of less than a dB. The 3-dB bandwidth of 60.4 nm without interposer is reduced to 39.5 nm, due to the smaller than ideal lens focal distance, as explained in the following.

Figure 8(a) shows the image of the packaged PIC with interposer and FA. After the FA and interposer were aligned to the GC pair on the PIC, UV-curable epoxy was dispensed onto the interposer attachment surfaces, that were then brought in contact with the PIC and the FA, after which the FA and interposer were realigned and the epoxy cured by UV light. Figure 8(b) shows the transmission spectra corresponding to FA coupling without (blue curve) and with bonded interposer (red curve), again divided by two to represent the ILs per optical port. After permanent attachment, the minimum loss was found to be 5.1 dB at a wavelength of 1604.3 nm with a 3-dB bandwidth of 38.8 nm. Comparing to direct FA coupling, the packaged PIC with interposer also has less than 1 dB excess ILs per optical port. The reduction of ILs compared to fiber-to-fiber experiments is attributed to the small beam transformation occurring inside the interposer, that may help here to better match the GC emission to the fiber mode.

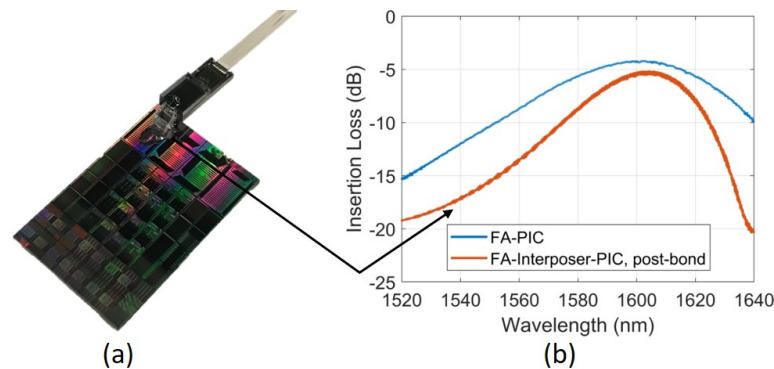


Figure 8. (a) Photograph of a packaged PIC with interposer and FA. (b) ILs per optical port for an FA coupled to the PIC via a GC without (blue curve) and with bonded interposer (red curve).

## 2.5 Grating coupler bandwidth

As reported in the previous section, for the first interposer designs a bandwidth reduction was observed compared to a GC directly coupled to an FA. However, this is rather unexpected as the interposer itself operates in a very wide wavelength range, covering multiple optical telecommunication bands. Moreover, the glass interposer is intended to act as a one-to-one imaging device, imaging the GC emission at the surface of the PIC to the fiber interface and vice versa.

Two aspects come into play here. One is the slightly too low focal length of the interposer lenses used here, which leads to the PIC and FA being placed slightly behind the focal plane of the interposer, since the distances to the lenses are fixed to 400  $\mu\text{m}$  by the lens recess. The other one is the well-known wavelength dependence of GC emission angles, predicted from diffraction.

Thus, a change in the wavelength leads to a change in the angle of the emitted light. Since the angle at which the receiving fiber is polished is kept constant, this leads to a mismatch to the fiber mode in k-space and thus to an increase in ILs, both when an interposer is used or not. This corresponds to the behavior seen when attaching a FA directly onto the PIC, shown by the blue dotted curve in Fig. 9. With an interposer that ideally images the GC output one-to-one onto the fiber edge, the same wavelength dependency would be expected. However, since the focal length of the lenses was chosen a bit too short, the GC emission is imaged at a point slightly before the fiber facet. Besides generating some excess insertion losses, this

also leads to a pivot effect in regards to where the light reaches the FA. Indeed, the image remains at the same point as the GC emission angle changes, however further propagation past this point leads to a wavelength dependent beam displacement at the FA. Compensating this on a wavelength specific basis is rather straightforward prior to permanent attachment, as the FA only needs to be translated in the plane of the attachment plane. This is shown in Fig. 9 for four different cases, where the alignment was repeated at different wavelengths for which an insertion loss similar and in some cases even better than the reference case was obtained at the alignment wavelength. Consequently, it is expected that the bandwidth reduction will disappear once the reoptimized lenses have been fabricated for the conjugated image planes to coincide with the attachment surfaces.

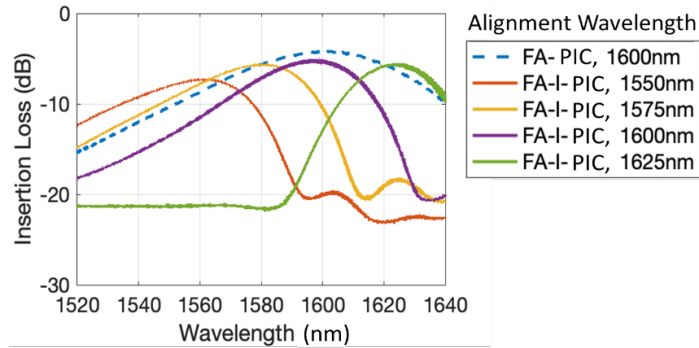


Figure 9. PIC-interposer-FA ILs for different alignment wavelengths.

### 3. EXTENDED FUNCTIONALITY

#### 3.1 Polarization splitting interposer configurations with integrated isolation

Due to both the increased cost of polarization maintaining fiber (PMF) itself, as well as the increased complexity of aligning its slow/fast axis to the polarization of the light during assembly, SMF fiber is usually preferred, even in very short distance optical connections. This does lead, however, to challenges related to polarization management, in particular when polarization sensitive interfaces such as GCs are being utilized.<sup>8</sup> Polarization splitting grating couplers<sup>9</sup> (PSGC), while allowing for coupling of both fiber polarizations, are also subjected to polarization dependent losses (PDL) resulting from the non-orthogonality of the two fiber polarizations preferentially coupled to one of its two output waveguides after projection onto the PIC surface. While substantial progress has been made in reducing their PDL, this typically requires high resolution lithography with anisotropic scatterers<sup>10</sup> not readily available in all foundry services. Other vertically emitting couplers do not split polarizations<sup>11</sup> and require additional on-chip devices to handle them.<sup>12</sup> Consequently, there are advantages to incorporate polarization management into the packaging solution if this does not significantly increase the package cost and complexity, as this may enable improvements of the overall link budget, of the PDL and of requirements placed on the lithography. Here, we propose an approach building on the interposer technology described above with very little added complexity by adding a polarization-beam-splitting (PBS) thin-film coating arranged in MacNeille configuration inside the interposer. Local deposition by shadow masking would remain compatible with batch-processing at the glass wafer level and thus not add substantial cost.

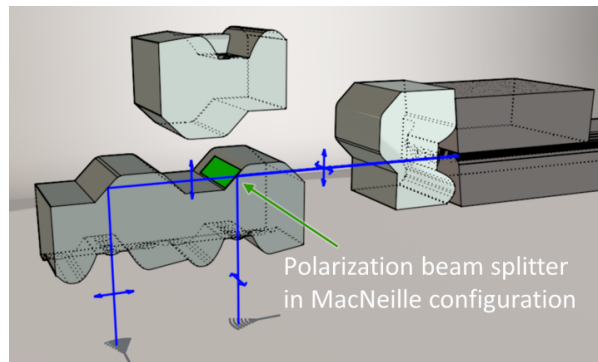


Figure 10. Extrusion drawing of a polarization splitting interposer configuration for side coupling. The beam path and electric field polarization are represented by blue arrows, the PBS coating by a green surface.

Figure 10 shows a CAD drawing of an interposer configuration that can be used to receive light from an SMF with the regular polarization-sensitive GCs widely adopted in SiP. The beam path corresponding to coupling in light from the side is represented in blue. The topmost interposer building block does not require a lens in this side-coupled configuration and can be replaced by a simpler filler that only features the two 45°-angled surfaces. In any case, it can be placed without requiring precise alignment in the direction perpendicular to the plane of the beam propagation, as it only serves to provide a homogeneous dielectric environment on both sides of the PBS and a medium in which the beam can propagate.

Blue arrows are overlaid on the beam path to represent the polarization of the electric field. When the light enters the assembly from an SMF embedded in the FA shown to the right, it gets collimated by the interposer lens and travels through the glass body. At the 45°-angled surface-coated internal facet, it is split into two beams with orthogonal polarizations. Separate lenses refocus the light onto the GCs placed on the PIC below, that are rotated such that the light reaches them with the appropriate polarization.

Similarly, top coupling can be realized by attaching the FA to the topmost building block, as shown in Fig. 11. In this case, the rightmost interposer is no longer required. While in this case the polarization arriving at the PIC is rotated by 90° for each of the optical interfaces, this can be easily adapted for by reorienting them.

These interposer configurations can be used to handle polarization at a receiver or to launch separate data streams at a polarization diverse transmitter. Similar challenges exist in coarse wavelength division multiplexed (CWDM) transceivers, since GCs have finite optical bandwidths and external (de-)multiplexer might thus be preferable. Such external package-based MUX-functionality is moreover unavoidable in transceiver solutions based on vertical cavity surface emitting lasers (VCSELs) and large area detectors (LADs)<sup>13</sup> and can be obtained by replacing the PBS coating by dichroic mirrors in the extrusion drawing shown in Fig. 10. Evidently, the interposer configuration would then benefit from an increased element count on the bottom plane, combining a larger number of dichroic mirrors in the beam path. This can be simply realized by dicing the glass wafer into larger blocks along the horizontal propagation axis. Four basic blocks can for example be transferred together to the PIC to handle four groups of wavelengths each fitting within the typical 25 nm wide 1-dB bandwidth of single polarization GCs.<sup>8,14</sup> The glass interposers can be further adapted to route the light with a different angle to or from individual grating couplers, depending on their center wavelength. This allows to further improve their coupling efficiency since fully optimized GCs either require a custom buried oxide (BOX) thickness or a custom emission angle.

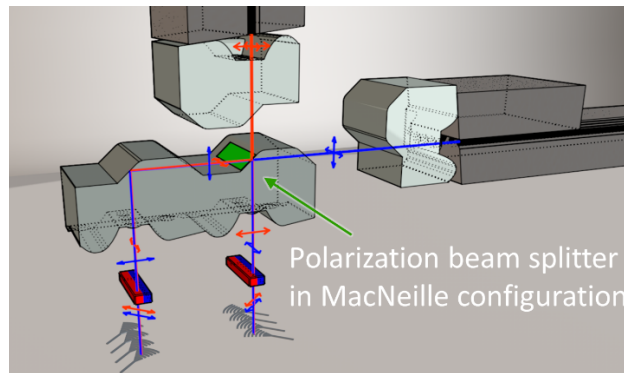


Figure 11. Extrusion drawing of interposer configurations for top and side coupling utilizing a 45° Faraday rotator placed on the PIC and in the beam path in between the GCs and the interposer. It forms an isolator together with the polarization selective beam routing of the PBS and the polarization selectivity of the GCs. The beam paths and corresponding polarizations are represented in blue and red for the side and top coupling configurations, respectively.

Back reflections are generally undesirable in optical communication systems and particularly problematic when they return to the emitting laser, due to resulting instabilities and laser emission coherence loss. While in some SiP transceiver solutions the laser is mounted in a micro-package already provided with optical isolation,<sup>15,16</sup> heterogeneous integration of lasers inside an SiP chip<sup>17,18</sup> in particular calls for an isolator at the output of the transmitter. Optical isolators typically make use of non-reciprocal Faraday rotators together with polarization selective elements such as birefringent materials. We combine the functionality of the polarization splitting interposer shown in Fig. 10 with latching garnets with a high Verdet constant attached as small dies onto the PIC on top of the GC. Due to their small size, with a few 100 μm to a side, they fit below the recess molded into the glass, see the extrusion diagram in Fig. 11. They can be cut to the adequate dimensions by using either laser cutting with high-power pulsed lasers<sup>19</sup> or with a conventional dicing saw, with the latter

requiring a remagnetization step after dicing, due to the high-level of induced vibrations. The small size of the garnet dies is essential to keep material costs low.

These garnets are commercially available with broadband antireflective (AR) coatings adapted to a garnet-air interface on the one side and a garnet-SiO<sub>2</sub> interface on the other, so that minimal additional ILs are obtained when they are attached to the PIC with a suitable index matched epoxy. Their thickness is adjusted so that together with the saturation remanence and the Verdet constant of the garnet a single light pass at the design wavelength leads to a 45° rotation of the polarization. To keep the compatibility with the PBS coating introduced above, the GCs are rotated by an additional 45° (Fig. 11). The depth of the recess in which the lenses are molded is adjusted to account for the beam path through the increased refractive index of the garnet, after which ray tracing simulations indicate an increase in ILs of less than 0.1 dB.

The optical isolation functionality is obtained from a combination of the PBS, the Faraday rotator and the polarization selectivity of the GCs. Reflected light returns to the GCs with the orthogonal polarization with which it was emitted. The light is then attenuated by an additional ~20 dB typical for the polarization sensitivity of standard single polarization GCs.<sup>8</sup>

### 3.2 Polarization beam splitting coating

We have developed a PBS coating matched to the utilized glass formed by a total of 19 alternately grown layers of SiO<sub>2</sub> and SiON, deposited on the 45 degree surface of the interposer. The nominal design features negligible insertion losses for the transmitted s-polarization (the unwanted reflection is below -35 dB). The p-polarization is almost entirely reflected with a residual transmission below -23 dB across the O-band.

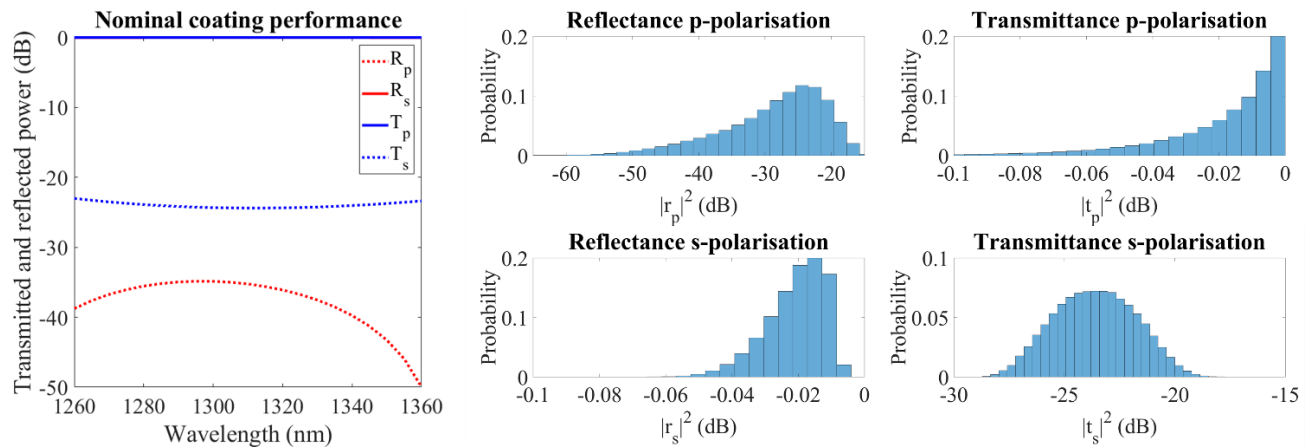


Figure 12. Left: Nominal coating performance in the O-band. Right: Monte Carlo simulations of the reflectance and transmittance of the SiO<sub>2</sub>-SiON PBS layer stack. 100k simulations at a wavelength of 1310 nm have parameters uniformly distributed across ±1° angle of incidence, ±0.02 refractive index and ±30 nm thickness.

To be able to better estimate the performance of the layer stack after fabrication imperfections are taken into account, Monte Carlo simulations are performed with the commercial software Lumerical STACK after comparing the nominal design results to our own transfer matrix calculations. The results of this analysis are shown in the right panel of Fig. 12. Conservative assumptions were considered for all parameters, for example the control over the angle of incidence that we can achieve in practice is below 0.1°.

In a similar fashion, dichroic coatings for wavelength splitting and combining can be realized, which would allow optimization of GCs and other usually wavelength-dependent integrated components towards higher performance/lower optical bandwidths. Since dichroic mirrors are fabricated on interposer facets defined by the glass molding process with tolerances below 0.1°, a very good reproducibility of their cutoff wavelength can be obtained.

### 3.3 Mode size transformation

Utilizing different lens types on the two sides of the interposer, with different focal distances and correspondingly adapted recess depths, enables a beam size transformation between the PIC or optical subassembly (VCSEL/LAD) and the fibers. This allows accommodating for example narrow aperture VCSEL and to reduce the beam size arriving at an LAD. In SiP, this also deconstrains the size of the beam that has to be generated or accepted by GCs. Highly efficient GCs with 0.9 dB peak insertion losses and a 1-dB bandwidth of 158 nm in the C-band have for example been designed with critical

dimensions compatible with the more advanced lithographic nodes.<sup>20</sup> However, they either require non-standard fibers with a small MFD of only 3.2  $\mu\text{m}$  or further transformation to the mode of a standard SMF-28 fiber, which can be implemented by the glass interposer technology described here.

### 3.4 Data rate scaling and co-packaged optics

The increasing demand for dense fiber connections seems to have no end in the near future. Emerging 800G modules require up to 16 fibers. Challenges related to fiber density will continue to rise as co-packaged optics are being rolled out, making it necessary to cram an ever growing number of fibers in a small space. While near-term commercial development focuses largely on edge coupled co-packaged optics, the pressure to increase fiber counts might lead to solutions in which fibers are routed out from the top of package, that can make use of the entire surface of a reticle to increase fiber count. We are currently developing interposer configurations based on a generalization of the top-FA-coupled configuration in Fig. 11 compatible with two-dimensional (2D) arrays of optical ports and compatible with external polarization control and wavelength multiplexing. These are based on a stack of only two isothermally molded glass pieces and (glass-)wafer-scale deposition of thin film coatings. The details of this solution are out of the scope of this proceedings paper, we are however preparing a demonstration with 32 parallel, polarization diverse transmitter and receiver pairs with 100 GBd compatible modulators and a potential aggregate bandwidth of up to 6.4 Tb/s if operated with PAM4 modulation, in which carriers are supplied by external laser diodes connected with non-PM fiber. The SiP die and the entire optical package fit in an area of 12 mm by 7.4 mm, so that a total bi-directional data rate of 51.2 Tb/s could be provided by an entire 25 mm by 30 mm reticle, corresponding to the I/O requirements of a 102.4 Tb/s datacom switch. Current optical I/O density is limited by the chosen 250  $\mu\text{m}$  pitch and the thickness of available FAs and could be scaled up further in the future. We are also currently working on glass-molded interposers compatible with dense edge coupling and external polarization control.

## 4. CONCLUSIONS

In summary, we have introduced highly scalable and flexibly utilized optical interposers fabricated by high-precision isothermal glass molding that can provide polarization handling, optical isolation and coarse wavelength multiplexing. They are compatible with low-rise side coupling and increased fiber density top coupling. Measurement results of the basic configuration enabling PIC coupling to fibers arriving from the side were presented. This validated base technology is being utilized to develop interposers with extended functionality and fiber count. Excess FA to PIC insertion losses of below 1 dB were experimentally shown for lenses produced on a glass wafer with over 1000 lenses. This paves the way for cost-effective wafer-level packaging solutions for both module and co-packaged optics form factors.

## ACKNOWLEDGEMENTS

The authors would like to acknowledge support by the German Ministry for Research and Education (BMBF) for project EFFICIENTlight (contract no. 13N14964).

## REFERENCES

- [1] Fuchs, E. R. H., Kirchain, R. E. and Liu, S., "The Future of Silicon Photonics: Not So Fast?," *J. Lightw. Technol.*, vol. 29, no. 15, pp. 2319-2326, 2011.
- [2] Masini, G., Capellini, G., Witzens, J., Gunn, C., "High-speed, monolithic CMOS receivers at 1550nm with Ge on Si waveguide photodetectors," in *Proc. IEEE Las. and Electro-Opt. Soc. Ann. Meet. Conf. (LEOS)*, ThU1 (2007).
- [3] Fatholouloumi, S. et al., "1.6Tbps Silicon Photonics Integrated Circuit for Co-Packaged Optical-IO Switch Applications," in *Proc. Opt. Netw. Comm. Conf. & Exhibit. (OFC)*, Art. ID T3H.1, 2020.
- [4] Chaqmaqchee, F. A. I. and Lott, J. A., "Impact of oxide aperture diameter on optical output power, spectral emission, and bandwidth for 980 nm VCSELs," *OSA Cont.*, vol. 3, no. 9, pp. 2602-2613, 2020.
- [5] Li, K., Chen, X., Hurley, J. E., Stone, J. S., Li, M.-J., "High data rate few-mode transmission over graded-index single-mode fiber using 850 nm single-mode VCSEL," *Opt. Expr.* 27(15), 21395-21404 (2019).
- [6] Nussbaum, P., Völkel, R., Herzig, H. P., Eisner, M., Haselbeck, S., "Design, fabrication and testing of microlens arrays for sensors and microsystems," *Pure Appl. Opt.* 6, 617-636 (2017).

- [7] Yin, S., Jia, H., Zhang, G., Chen, F. and Zhu, K., “Review of small aspheric glass lens molding technologies,” *Front. Mech. Eng.* 12(1), 66–76 (2017).
- [8] Marchetti, R., Lacava, C., Carroll, L., Gradkowski, K., and Minzioni, P., “Coupling strategies for silicon photonics integrated chips,” *Photon. Res.* 7(2), 201-239 (2019).
- [9] Gunn, L. C., Pinghet, T. J., Rattier, M. J., Witzens, J., “Polarization splitting grating coupler,” US Patent US7006732B2 (2003).
- [10] Chen, B., Zhang, X., Hu, J., Zhu, Y., Cai, X., Chen, P., and Liu, L., “Two-dimensional grating coupler on silicon with a high coupling efficiency and a low polarization-dependent loss,” *Opt. Expr.* 28(3), 4001-4009 (2020).
- [11] Rong, H., Gan, O., Srinivasan, P., Barkai, A., Hsieh, I.-W. A., Krishnamoorthy, M., Na, Y.C. N., “Vertical optical coupler for planar photonic circuits,” US Patent US9658396B2 (2011).
- [12] Xie, C., Zou, X., Li, P., Yan, L. and Pan, W., “Ultracompact silicon polarization splitter-rotator using a dual-etched and tapered coupler,” *Appl. Opt.* 59(30), 9540-9547 (2020).
- [13] Wang, B., Sorin, W. V., Rosenberg, P., Kiyama, L., Mathai, S., and Tan, M. R. T., “4x112 Gbps/Fiber CWDM VCSEL Arrays for Co-Packaged Interconnects,” *J. Lightwav. Technol.* 38(13), 3439-3444 (2020).
- [14] He, L., Liu, Y., Galland, C., Lim, A. E.-J., Lo, G.-Q., Baehr-Jones, T. and Hochberg, M., “A High-Efficiency Nonuniform Grating Coupler Realized With 248-nm Optical Lithography,” *IEEE Photon. Technol. Lett.* 25(14), 1358–1361 (2013).
- [15] Narasimha, A., *et al.*, “An ultra low power CMOS photonics technology platform for H/S optoelectronic transceivers at less than \$1 per Gbps,” in *Proc. Opt. Fib. Conf. (OFC)*, OMV4 (2010).
- [16] Snyder, B., Corbett, B., and O'Brien, P., “Hybrid integration of the wavelength-tunable laser with a silicon photonic integrated circuit,” *J. Lightw. Technol.* 31, 3934-3942 (2013).
- [17] Stankovic, S., Jones, R., Sysak, M. N., Heck, J. M., Roelkens, G., and Van Thourhout, D., “Hybrid III-V/Si Distributed-Feedback Laser Based on Adhesive Bonding,” *IEEE Photon. Technol. Lett.* 24(23), 2155-2158 (2012).
- [18] Shin, D., Cha, J., Kim, S., Shin, Y., Cho, K., Ha, K., Jeong, G., Hong, H., Lee, K., and K. H.-K., “O-band DFB laser heterogeneously integrated on a bulk-silicon platform,” *Opt. Expr.* 26(11), 14768-14774 (2018).
- [19] Kalupka, C., Schmalstieg, M. and Reininghaus, M., “Ultrashort Pulse Processing of Transparent Ceramics: The Role of Electronic and Thermal Damage Mechanisms,” *J. Las. Micro/Nanoeng.* 13(2), 126-130 (2018).
- [20] Melati, D., Dezfouli, M. K., Grinberg, Y., Schmid, J. H., Cheriton, R., Janz, S., Cheben, P., Xu, D., “Design of Compact and Efficient Silicon Photonic Micro Antennas with Perfectly Vertical Emission,” *J. Select. Top. Quant. Electron.* 27(1), 8200110 (2021).